Surface intermediates in the catalytic reaction of NO + H_2 on Rh studied by method of interacting bonds calculations

A.R. Cholach and N.N. Bulgakov

Boreskov Institute of Catalysis, prospect Akademika Lavrentieva 5, 630090 Novosibirsk, Russia

Received 24 October 1996; accepted 2 September 1997

The semi-empirical method of interacting bonds was used to clarify the mechanism of oscillatory behavior of the catalytic system (NO + H_2)/Rh. Various rhodium planes and surface defect regions were characterized by the strength of the nitrogen bond to the surface, the stability of the adsorbed NH_n species ($n = 0, 1, 2, 3$), and the reactivity of NH_n species towards hydrogen. Calculations admit the earlier suggested reaction mechanism, which attributes the surface wave propagation to the intermediate formation of NH_a species. The activity of the rhodium surface in oscillations is expected to increase in a row of planes: (100) < (111) < (335). The activity of Rh(335) single crystal in the *reaction rate* oscillations is probably governed by the presence (in contrast to ideal terraces) of gradient and broad range of the reaction intermediate properties.

Keywords: NO hydrogenation, oscillations, rhodium, semi-empirical calculations, surface species

1. Introduction

Spatio-temporal oscillations were found to proceed in the course of the catalytic NO + H_2 reaction over a Rh tip studied by field emission microscopy (FEM) [1]. The vacancy mechanism was suggested to explain the observed phenomena. However, the feedback mechanism was not very clear, because there were no reasons to start a certain wave instead of the steady state reaction proceeding on the nearly clean surface which is formed after the wave propagation. The oscillation mechanism proposed in ref. [2] includes the reversible hydrogenation of the atomically adsorbed nitrogen N_a, as shown in scheme 1. It was concluded from the following points: (a) Thermal desorption spectra obtained after the special sample treatment in NO–H_2 mixture reveal the simultaneous H_2 and N_2 desorption with H_2 : N_2 ratio close to unity. The hydrogen desorption temperature was much higher than that of H_2 desorption from the clean Rh surface. (b) The feedback mechanism looks clear: the wave propagation is just an adding of the alternative reaction pathway (through the NH_a recombination) whenever the necessary N_a coverage is reached. It is followed by restoring of N_a coverage in the course of the NO + H_2 reaction. (c) The suggested mechanism is in line with other experimental data on $NH_{x(ads)}$ formation on rhodium [19–21]. Besides, in ref. [2] it has been shown that the grain boundaries are responsible for the surface wave initiation. It was found also, that the (100) and probably (111) planes of the Rh tip are inactive in the surface wave propagation, whereas all the rest surface of the Rh tip is active [1,2]. Moreover, Rh(335) single crystal turned out to be active in the sustained *reaction rate* oscillations [3,4].

The present study aims at analyzing the adsorption system NH_n/Rh (where $n = 0, 1, 2, 3$) using the semi-empirical calculations by the method of interacting bonds (MIB) in order: (a) to test if the mechanism of stable spatio-temporal oscillations, followed by FEM [2,3], guides the catalytic reaction NO + H_2 on Rh; (b) to elucidate the role of surface defects in oscillations; (c) to find out why rhodium (100) and (111) surfaces are not (or nearly not) involved in the surface wave propagation; (d) to compare the properties of Rh surfaces: (111), (100)

(1)	$H_{2(gas)} + 2*$	$\rightleftharpoons 2H_{ads}$	+	18.6 kcal		[16,17]
(2)	$NO_{gas} + *$	$\rightleftharpoons NO_{ads}$	}			
(3a)	$NO_{ads} + *$	$\rightarrow N_{ads} + O_{ads}$	} +	26.3 kcal		[18,MIB]
(3b)	$O_{ads} + 2H_{ads}$	$\rightarrow H_2O_{gas} + 3*$	+	11.3 kcal		[11,16–18]
(**4**)	$\mathbf{N_{ads}} + \mathbf{H_{ads}}$	$\rightarrow [\mathbf{NH_{ads}}] + *$				
	$[\mathbf{NH_{ads}}]$	$\rightarrow \frac{1}{2}\mathbf{N_{2(gas)}} + \frac{1}{2}\mathbf{H_{2(gas)}} + *$				
	or					
	$\mathbf{2[NH_{ads}]}$	$\rightarrow \mathbf{N_{2(gas)}} + \mathbf{H_{2(gas)}} + \mathbf{2*}$				
(5)	$NH_{ads} + 2H_{ads}$	$\rightarrow NH_{3(gas)} + 3*$				
(6)	$2N_{ads}$	$\rightarrow N_{2(gas)} + 2*$	+	26–30 kcal	for Rh(111)	
				39.4 kcal	for Rh(100)	[14,25]

Scheme 1. Sequential steps of the catalytic reaction NO + H_2 on Rh according to ref. [2]. * vacant adsorption site. To the right are indicated the references of the experimental or present MIB data regarding the step heats.

(inactive in FEM-oscillations) and (335) = [4(111) ×(100)] (active in FEM-oscillations and in the reaction rate oscillations) regarding the stability and activity of the intermediate surface species. For this purpose we have calculated the formation enthalpies of NH_n species for the various coordinations of the nitrogen atom and surface Rh atoms, and respective coverage on the (111), (100) and (335) planes. We took in our calculations for the $NH_{n(ads)}$ particle, that the n hydrogen atoms are bound to the nitrogen atom only, not to the surface Rh atoms.

2. Theory

2.1. The principle of the method of interacting bonds

The method of interacting bonds [5] considers multiatomic systems described as a set of two-center bonds. Each ith bond is characterized by an empirical parameter E_i similar to the well known bond energy by its physical sense. Usually E_i depends only on the type of atoms forming the bond. Beside, for each ith bond we introduce a variable bond coefficient ν_i ($0 < \nu_i < 1$), whose value and thus contribution of the ith bond to the total energy of the system is characterized by the whole system structure. We also account for the interaction (repulsion) between the ith and kth bond sharing an atom. This interaction is characterized by an empirical parameter Δ_{ik} depending on the type of the atom involved. Atomization energy is written as

$$H_a = \sum_i E_i \nu_i (2 - \nu_i) - \sum_{i>k} \sum \Delta_{ik} \nu_i \nu_k \,.$$

Bond coefficients ν_i are found then from the maximum of the H_a value (energy minimum):

$$\partial H_a / \partial \nu_i = 0 \,.$$

Practice shows that one can apply the method to systems of various chemical origin (oxides [5–7], sulfides [8,9], metals [10], etc.) The simplicity of the method allows us to consider rather complex structures (surfaces, interfaces, extended defects of solids, etc.) without any simplifying assumptions.

2.2. Choice of parameters

Table 1 enlists parameters E_i and Δ_i used in our calculations. Parameters 1–5 seem correct, because they were determined from reliable experimental data and tested numerously in the previous MIB calculations [5,10,12,13]. As Rh does not form nitrides and is inactive in the nitrogen dissociative adsorption, there are no reference experimental data providing the direct calculation of parameter E_{RhN}. It was estimated from $E_{RhO} = 106$ kcal, which was calculated from the known structure and energy of oxide Rh_2O_3 formation, since $E_{(M-O)}$ of transition metals usually exceeds $E_{(M-N)}$ by ~ 10 kcal [5,10]. According to our calculations, the E_{RhN} variation in a range of 90–105 kcal does not qualitatively affect the deduction. However, we paid special attention to the verification of the used E_{RhN} value.

3. Results and discussion

3.1. Atomically adsorbed nitrogen

The properties of N_a on rhodium (100), (111), and (110) surfaces were studied by MIB first to try and test the parameters action. On the other hand, atomic nitrogen is one of the intermediates in the NO + H_2 reaction that is the matter of our interest. Tables 2 and 3 give the heats of N_a and NH_a formation at various nitrogen atom coordination numbers with respect to the surface Rh atoms, and various coverages. All the Q values at zero coverage actually coincide with the respective Q values at $\Theta = 0.25$ ML (monolayer). As expected, the heat of nitrogen adsorption rises as the coordination number increases, and coverage decreases. However, it remains negative (endothermic) even for NM_5, whose formation seems very unprobable due to steric reasons. Thus, multi-coordinated adsorption states are favored: $(H)NM_3$ and $(H)NM_4$ for (111) and (100) surfaces, respectively. Note, the nitrogen bond on (100) plane is by ca. 10–12 kcal/(mol N_a) stronger than that on (111) plane. One can estimate the diffusion activation barrier E_{dif} as a difference between the formation heats of various neighbor N_a states presented in tables 2 and 3. The

Table 1
Bond parameters used in MIB calculations

No.	Parameter	Value (kcal/mol)	Way of determination
1	E_{RhRh}	79.6	from Rh sublimation heat [11]
2	Δ_{Rh}	18.5	from empirical ratio $E_{MM}/\Delta_M = 4.3$ [10]
3	E_{NH}	139.4	from NH_3 atomization heat [12]
4	Δ_N	75	according to ref. [10]
5	E_{RhO}	106	from heat of Rh_2O_3 formation [13]
6	E_{RhN}	97	from empirical ratio between E_{MO} and E_{MN} [10]

Table 2
Heat of formation of N_a and NH_a (kcal/mol) at shown coverage and various orders of nitrogen atom bonding to the Rh(111) surface according to reactions: $\frac{1}{2}N_{2(gas)} + \frac{1}{2}H_{2(gas)} \rightarrow NH_a + Q_{NH}$ and $\frac{1}{2}N_{2(gas)} \rightarrow N_a + Q_N$

Adsorption state	Q_{NH}	Q_N	Schematic top view [a]
(H)NM_1			
$\Theta = 0.25$	−14.5	−63.6	
$\Theta = 1.00$	−13.8	−61.6	
(H)NM_2			
$\Theta = 0.25$	−8.2	−40.7	
$\Theta = 1.00$	−8.5	−41.9	
(H)NM_3			
$\Theta = 0.25$	−4.7	−28.8	
$\Theta = 1.00$	−5.5	−31.5	

[a] ○ surface rhodium atom M, ● adsorbed nitrogen atom or NH particle.

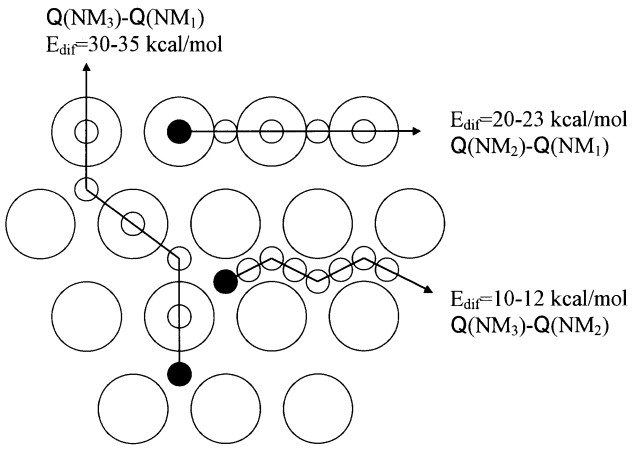

Figure 1. Atomic nitrogen diffusion activation barriers E_{dif} over the Rh(111) surface. Energy intervals are due to the respective bond strength difference at high and low coverage. Polygonal lines with arrows: schematic diffusion paths with different intermediate nitrogen atom bonding to the surface; large open circles: surface Rh atoms; small black circles: initial N_a positions; small open circles: intermediate N_a positions in the course of diffusion. See designations in table 2.

way of E_{dif} determination is demonstrated in figures 1 and 2, where the possible paths of N_a diffusion over (111) and (100) planes are presented. Figures 1 and 2 show that the lowest E_{dif} values correspond to N_a transition from three- to two-bound state on the (111) plane, and from four- to two-bound state on the (100) plane.

Nitrogen adsorption states on (1×1) and reconstructed (2×1) rhodium (110) surfaces have been considered as well in order to make a comparison with available experimental data [22–24]. Surface energies were found to be 1520 and 1930 mJ/m^2 for (1×1) and (2×1) structures, respectively. Therefore, a clean rhodium (110) surface with (1×1) structure is favored, that is, actually takes place [22,24]. The lower symmetry of both surfaces in comparison with the (111) and (100) ones results in multiple ways of nitrogen atom bonding to the surface, as presented in tables 4 and 5. The adsorption heat at the most favorable state (1) on the (1×1) surface is lower than that on the reconstructed (2×1) one. This is in agreement with the properties and suggested structures of experimentally observed β_1 and β_2 N_a states shown in figures 3a and 3b [22,23]. Moreover, Rh–Rh bond coefficients of the β_1 state were found as follows:

$\nu_{(A-B)}$	$\nu_{(A'-B)}$	$\nu_{(A-C)}$	$\nu_{(A'-C)}$
0.3047	0.3680	0.3211	0.3806

Table 3
Heat of formation of N_a and NH_a (kcal/mol) at shown coverage and various coordination numbers of nitrogen atom bonding to the Rh(100) surface according to reactions: $\frac{1}{2}N_{2(gas)} + \frac{1}{2}H_{2(gas)} \rightarrow NH_a + Q_{NH}$ and $\frac{1}{2}N_{2(gas)} \rightarrow N_a + Q_N$

Adsorption state	Q_{NH}	Q_N	Schematic [a] top view
(H)NM_1			
$\Theta = 0.25$	−12.9	−60.1	
$\Theta = 1.00$	−12.7	−59.6	
(H)NM_2			
$\Theta = 0.25$	−6.4	−37.5	
$\Theta = 1.00$	−7.0	−39.4	
(H)NM_4			
$\Theta = 0.25$	−0.1	−17.4	
$\Theta = 1.00$	−1.6	−22.1	
(H)NM_5			
$\Theta = 0.25$	0.4	−14.5	

[a] ○ surface rhodium atom M, ● adsorbed nitrogen atom or NH particle.

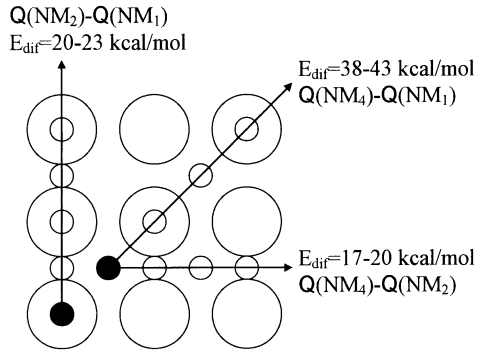

Figure 2. Atomic nitrogen diffusion activation barriers E_{dif} over the Rh(100) surface. Energy intervals are due to the respective bond strength difference at high and low coverage. Polygonal lines with arrows: schematic diffusion paths with different intermediate nitrogen atom bonding to the surface; large open circles: surface Rh atoms; small black circles: initial N_a positions; small open circles: intermediate N_a positions in the course of diffusion. See designations in table 3.

Table 4
Heats of $N_{2(gas)}$ adsorption to various atomic N_a states on Rh(110)-(1 × 1) surface [a]

	*i*th N_a state							
	1	$2^{(lb)}$	3	$4^{(sb)}$	$5^{(lb)}$	$6^{(sb)}$	7	8
number of bonds								
A–N and/or A′–N	2	2	1	2	2	2	1	0
B–N	2	1	1	1	0	0	0	1
Q_i (kcal/(mol N_a))	−21.7	−27.6	−40.1	−25.6	−37.4	−34.3	−57.9	−72.0

[a] A, A′ – rhodium atoms of the top layer, and B – rhodium atom of the second layer as shown in figure 3a; Q_i – heat of adsorption: $\frac{1}{2}N_{2(gas)} \rightarrow N_a + Q_i$; lb – long bridge state; sb – short bridge state. Note, the most favorable state 1 corresponds to the β_1 state shown in figure 3a.

where $\nu_{(i-j)}$ corresponds to the bond between the *i*th and *j*th rhodium atoms shown in figures 3a and 3b.

These data mean that rhodium atoms A are significantly weaker bound to second and third layers in comparison with A′ atoms, because the $\nu_{(i-j)}$ value actually stands for the bond strength between *i*th and *j*th atoms. This is in line with the "buckled" position of Rh atoms bound to nitrogen atoms of β_1 state according to ref. [22].

The similar to above estimations of the nitrogen atom diffusion barrier give 14.5 kcal/(mol N_a) for β_1 state as a difference of $(Q_4 - Q_3)$ from table 4, and 14.1 kcal/(mol N_a) for β_2 state as a difference of $(Q_3 - Q_2)$ from table 5. It worth noting that the calculated E_{dif} values listed in table 6 are approximately half as large as nitrogen desorption energies found for the respective rhodium surfaces. This may relate to the necessity to excite and move two N_a atoms in order to ensure N_2 desorption. Note, that both considered β states on the (110) plane show the tendency to reconstruct the surface at elevated temperatures [22–24]. So, the calculated properties of clean and nitrogen covered Rh(110) surfaces look qualitatively correct, but we have to be careful in comparison of E_{dif} and E_{des} in this case. Summing it up, one can conclude that our Rh–N bond parameter is quite reliable.

3.2. Reaction intermediates on Rh(100) and Rh(111) surfaces

NO + H_2 reaction on polycrystalline Rh was suggested to proceed as shown in scheme 1 [2]. Numerous experimental data on the adsorption and dissociation of NO and H_2, high activity of O_a towards hydrogen as well as high exothermicity of steps 1–3 testify to their easiness. The next step of the N_a hydrogenation followed by the recombination of NH_a species was the ground for interpreting the nature of surface waves observed by FEM [2]. However, there is no direct experimental evidence for the intermediate NH_a formation in the course of oscillations, so we paid particular attention to the analysis of this possibility by MIB.

Figure 4 presents the heats of NH_a formation from nitrogen and hydrogen at various bond parameters E_{RhN} versus the coverage on (111) and (100) surfaces. In both cases the heat of NH_a formation decreases as the coverage increases. Since the heat value is actually a measure of NH_a stability, the stability of NH_a species on the (100) surface is by 4–5 kcal higher in comparison with the (111) one. On the other hand, figure 5 shows that coverage increase provides a growing exothermicity of the adsorbed nitrogen hydrogenation yielding NH_a. The heat of this step is by 6–7 kcal lower on face (100) than on face (111). Considering this value as a measure of N_a activity towards H_a, one can conclude that the (111) plane should be appreciably more active than the (100) one.

According to our calculations, the steps of further NH_a hydrogenation resulting in $NH_{2(a)}$ and $NH_{3(a)}$ species formation are endothermic, as shown in table 7. Moreover, the values of the bond coefficients $\nu_{(Rh-N)}$ for

Table 5
Heats of $N_{2(gas)}$ adsorption to the various atomic N_a states on Rh(110)-(2 × 1) surface [a]

	*i*th N_a state												
	1	2	3	4	5	6	7	8	9	10	11	12	13
number of bonds													
A–N	2	2	1	1	1	0	2	1	0	0	1	0	0
B–N	2	1	1	1	2	2	0	0	2	1	0	1	0
C–N	0	0	0	1	1	1	0	1	0	1	0	0	1
Q_i (kcal/(mol N_a))	−13.1	−19.2	−33.3	−24.3	−18.5	−31.2	−29.1	−34.8	−42.1	−43.2	−51.7	−63.2	−64.7

[a] A, B, C – rhodium atoms of the top, second, and third layer, respectively, as shown in figure 3b; Q_i – heat of adsorption: $\frac{1}{2}N_{2(gas)} \rightarrow N_a + Q_i$. Note, the most favorable nitrogen state 1 corresponds to the β_2 state shown in figure 3b.

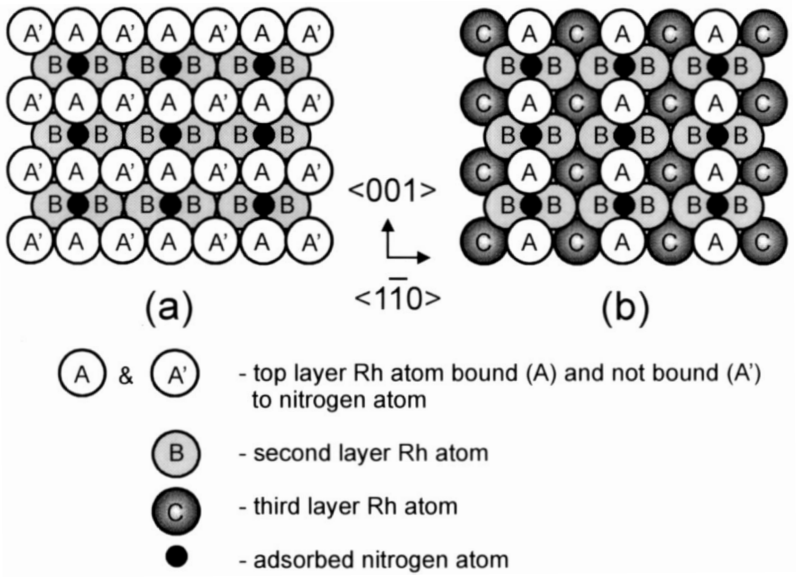

Figure 3. The optimum structure of the nitrogen adsorbed layer on the Rh(110) surface suggested in refs. [22,23] for β_1 state (a) and β_2 state (b).

$NH_{3(a)}$ are negative, in contrast to other cases. It means that this particle is not stable from the viewpoint of MIB. The formation of $NH_{n(a)}$ species from $N_{2(gas)}$ and $H_{2(gas)}$ is exothermic. However, NH_a species formation is characterized by the maximum Q_1 value. Hence, this particle is the favorable surface state among the products of the sequential hydrogenation of N_a in adsorbed layer.

Thus, the calculations show: (a) the hydrogenation of N_a yielding NH_a species on the rhodium surface is quite possible; (b) the buildup of N_a coverage promotes this process, and at the same time decreases the stability of NH_a species being formed. It is consistent with the suggested reaction scheme, assuming the "turn-on" of a new route of nitrogen removal from the surface at some critical nitrogen coverage, i.e. the formation and recombination (and/or decomposition) of NH_a species, that is responsible for the observed surface wave [2]; (c) the Rh(100) surface shows the more stable state of adsorbed nitrogen and the lower N_a activity to hydrogen in comparison with the (111) surface. Hence, we can expect the lower activity of the (100) plane in the surface wave propagation as compared to the (111) one.

Table 6
Calculated activation barriers E_{dif} for N_a diffusion over Rh surfaces compared to the experimental values of the respective nitrogen desorption energies E_{des}

	Surface structure			
	(100)	(111)	(110)	
			(1 × 1)	(2 × 1)
E_{dif} (kcal/(mol N_a))	17–20	10–12	14.5	14.1
E_{des} (kcal/(mol N_2))	39.4	26–30	27.5	28.2
references	[25]	[14]	[22]	

3.3. The peculiarity of surface defects

A surface defect like grain boundary can be characterized by the presence of the surface metal atoms, whose number of nearest neighbor surface atoms differs from the terrace one. We have accepted this consideration to elucidate why the defects are active in the surface wave initiation in the course of the self-sustained oscillations

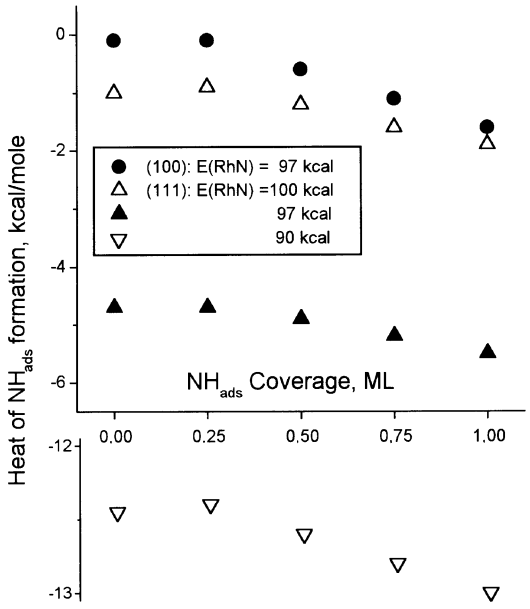

Figure 4. Heats of reaction $\frac{1}{2}H_{2(gas)} + \frac{1}{2}N_{2(gas)} \rightarrow NH_a + Q$ versus coverage of Rh(111) and Rh(100) surfaces at shown values of the E_{RhN} parameter.

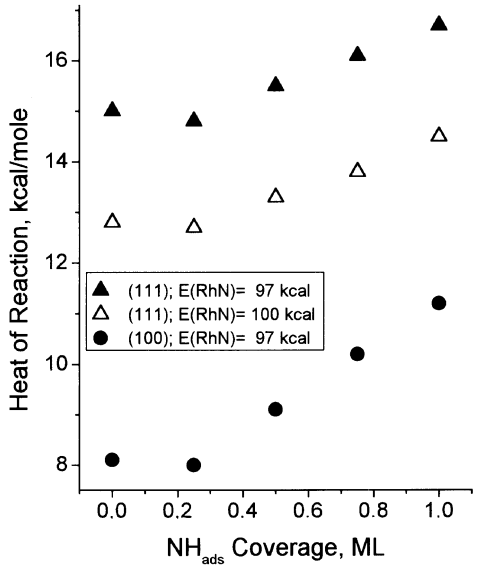

Figure 5. Heats of reaction $N_a + H_a \rightarrow NH_a + Q$ versus coverage of Rh(111) and Rh(100) surfaces at shown values of the E_{RhN} parameter.

observed by FEM [2]. Figure 6 shows the heat of NH_a formation as a function: of coverage for (111) terrace Rh atoms (fixed surface coordination number is 6); of surface coordination number at constant NH_a coverage of 0.5 ML. According to figure 6, reaction heat near the defect region varies over a much wider range in comparison with the ideal terrace (111). Therefore, it provides a wider spectrum of nitrogen bond strength to the surface and N_a activity towards hydrogen. Thus, the wave initiation at the surface defect region is preferable in comparison with the terraces because the adsorbed hydrogen can "choose" here the N_a state with the optimum bond strength and activity.

Table 7
Heats of sequential hydrogenation of atomically adsorbed nitrogen (Q_1, kcal/mol), and heats of $NH_{n(a)}$ formation from gaseous nitrogen and hydrogen (Q_2, kcal/mol) on rhodium (111) and (100) planes according to reactions: $H_a + NH_{(n-1)a} \rightarrow NH_{n(a)} + Q_1$ and $\frac{1}{2}nH_{2(gas)} + \frac{1}{2}N_{2(gas)} \rightarrow NH_{n(a)} + Q_2$

	Product particle			Coverage	Plane
	NH_a $n=1$	$NH_{2(a)}$ $n=2$	$NH_{3(a)}$ $n=3$		
Q_1	11.4	−2.7	−13.0 $\nu_{(Rh-N)} < 0$	$\Theta = 0.25$	Rh(111)
	12.0	−2.5	−12.9 $\nu_{(Rh-N)} < 0$	$\Theta = 0.50$	
Q_2	0.1	6.7	3.0	$\Theta = 0.25$	
	−0.2	6.6	3.0	$\Theta = 0.50$	
Q_1	4.6	−6.2	−14.6 $\nu_{(Rh-N)} < 0$	$\Theta = 0.25$	Rh(100)
	5.6	−5.8	−1.45 $\nu_{(Rh-N)} < 0$	$\Theta = 0.50$	
Q_2	5.1	8.2	2.9	$\Theta = 0.25$	
	4.6	8.1	2.9	$\Theta = 0.50$	

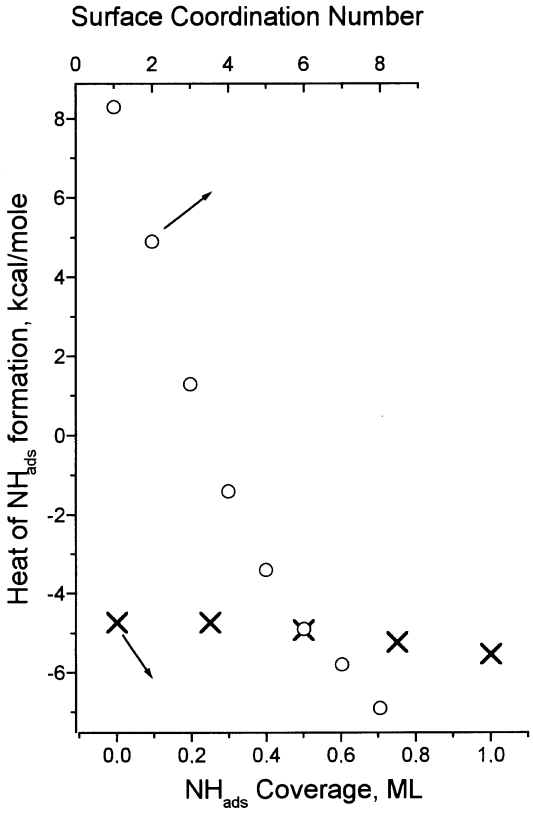

Figure 6. Heats of reaction $\frac{1}{2}H_{2(gas)} + \frac{1}{2}N_{2(gas)} \rightarrow NH_a + Q$ on the Rh(111) surface: bottom and left axes – as a function of coverage; top and left axes – as a function of coordination number of the surface Rh atoms.

3.4. NO + H_2 reaction on Rh(335) surface

To our knowledge, the reaction of $NO + H_2$ on Rh(335) single crystal is the only catalytic system where true experimental reference data proving the sustained reaction rate oscillations on rhodium surface are obtained [3,4]. So, it seems intriguing to analyze this surface using MIB, as we did for (111) and (100) planes. Surface $(335) = [4(111) \times (100)]$ comprises terraces (111) and steps (100), as shown in figure 7. The surface exhibits seven different adsorption sites, where the strongly bound nitrogen states can be formed. All the states were characterized by the heat of $N_{2(gas)}$ adsorption (N_a bond strength), the heat of NH_a formation from the gaseous nitrogen and hydrogen (i.e., stability of NH_a species) and heat of nitrogen hydrogenation in the adsorption layer (i.e., activity of N_a towards H_a) presented in table 8. For simplicity, we regard in our calculations surface coverage as a "linear" monolayer with respect to the adsorption species considered. The nitrogen atom in all the adsorbed species was assumed to be in three- and four-bound states on terrace and step, respectively. As one could expect from the surface structure, the properties of the (335) plane are a combination of properties of (111) and (100) planes (see tables 2–4). Note, however, some important peculiarities:

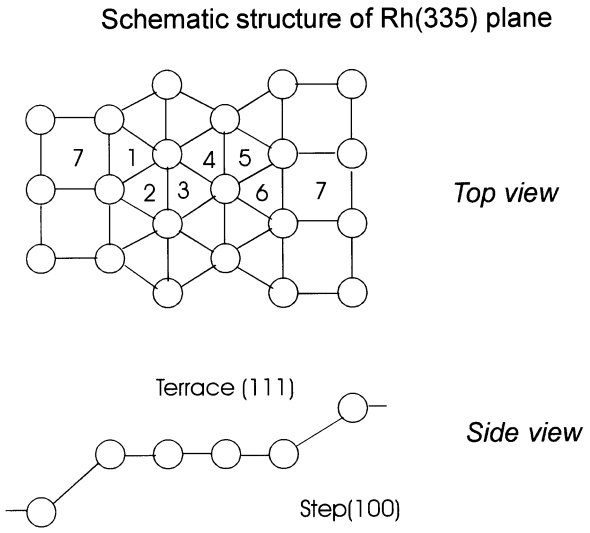

Figure 7. Schematic top and side views of the ideal Rh(335) plane.

(1) As table 8 evidences, there is a gradient of surface state properties in moving along the terrace from the step bottom to the top of the next step. In experiment it may result in facilitating the propagation of surface wave, which can start at some optimum surface site.

(2) The (335) surface exhibits a broad spectrum of stability and activity of N_a and NH_a. The characteristic energy interval for NH_a formation (Q_2 values from table 8) is 4.5 kcal. One can compare it with the similar intervals of 1–2 kcal for (111) and (100) surfaces (figure 4), and of ca. 15 kcal for the surface defect (figure 6). So, in this aspect Rh(335) surface takes up an intermediate position between the above considered planes and surface defect. Therefore, the surface wave initiation on this plane should be easier being compared to the ideal (111) and (100) planes. We suppose that these peculiarities of the Rh(335) surface are responsible for its activity in the self-sustained oscillations of the NO + H_2 reaction rate.

The present calculations are consistent with the recent experimental data on the self-sustained rate oscillations of NO + H_2 reaction over Rh(533) single crystal [4]. The authors [4] attribute the key role in oscillations to the accumulation of atomic nitrogen on the surface, as we do. They also observed a delay of N_2 production with respect to NH_3 production during the oscillations. To see this, if the Rh surface is saturated with N_a, then the step of full N_a hydrogenation in scheme 1 will be favored in comparison with the case of low N_a coverage. Summing up the present results we can expect the increasing of the rhodium activity in oscillatory behavior in the NO + H_2 reaction in the following row of planes: (100) < (111) < (335). This activity row is in agreement with the experimentally observed data: the (100) plane is inactive both in the surface wave propagation and in the macroscopic reaction rate oscillation [1,2,25], in contrast to the (335) plane [2–4]. The (111) plane takes an intermediate position: it reveals a low activity in the surface wave propagation [1,2], and irregular unstable reaction rate oscillations only ([26,27] – these references became available when the present paper had been submitted for publication).

Table 8
Heats of reactions calculated for various adsorption sites of Rh(335) surface shown in figure 7 (kcal/mol): $\frac{1}{2}N_{2(gas)} \rightarrow N_a + Q_1$, $\frac{1}{2}N_{2(gas)} + \frac{1}{2}H_{2(gas)} \rightarrow NH_a + Q_2$, $N_a + H_a \rightarrow NH_a + Q_3$

	Adsorption site no.						
	7	1	2	3	4	5	6
Q_1	−20.8	−25.3	−28.0	−30.4	−30.0	−30.6	−31.4
Q_2	−1.4	−2.7	−3.9	−5.3	−5.1	−5.4	−5.9
Q_3	10.1	13.9	14.8	15.8	15.6	15.9	16.2

4. Conclusion

The present calculations performed within the method of interacting bonds lead us to the following conclusions:

(1) MIB admits the suggested earlier mechanism of NO + H_2 reaction over rhodium (scheme 1), which attributes the observed surface waves to intermediate formation and recombination and/or decomposition of the NH_a species.

(2) The expected activity in oscillations of the studied rhodium planes increases in a row of planes: (100) < (111) < (335), which is in agreement with the known experimental data; it is governed by the respective increasing of N_a activity towards hydrogen, decreasing of the NH_a species stability, and the easiness of the surface wave initiation.

(3) The activity of defects in the surface wave initiation can result from the broader range of N_a activity towards hydrogen, as compared to ideal terraces.

(4) The activity of the Rh(335) single crystal in NO + H_2 reaction rate oscillations is probably governed by the presence of a broad range and gradient of the properties of intermediate surface states, which can appear in the course of reaction.

Acknowledgement

One of us (ARC) appreciates the financial support from the Grant of INTAS 93-0964, and the Russian Foundation for Fundamental Studies (Project 96-03-33211).

References

[1] M.F.H. van Tol, A. Gielbert and B.E. Nieuwenhuys, Catal. Lett. 16 (1992) 297.

[2] A.R. Cholach, M.F.H. van Tol and B.E. Nieuwenhuys, Surf. Sci. 320 (1994) 281.
[3] N.M.H. Janssen, B.E. Nieuwenhuys, M. Ikai, K. Tanaka and A.R. Cholach, Surf. Sci. 319 (1994) L29.
[4] N.M.H. Janssen, P.D. Cobden, B.E. Niewenhuys, M. Ikai, K. Mukai and K. Tanaka, Catal. Lett. 35 (1995) 155.
[5] N.N. Bulgakov, Yu.A. Borisov and V.V. Popovskii, Kinet. Catal. USSR 14 (1973) 395.
[6] N.N. Bulgakov, V.Yu. Aleksandrov and V.V. Popovskii, React. Kinet. Catal. Lett. 4 (1976) 473.
[7] N.N. Bulgakov, V.Yu. Aleksandrov and V.V. Popovskii, React. Kinet. Catal. Lett. 8 (1978) 53, 59, 65.
[8] Yu.I. Yermakov, A.N. Startsev, V.A. Burmistrov, O.N. Shumilo and N.N. Bulgakov, Appl. Catal. 18 (1985) 33.
[9] N.N. Bulgakov and A.N. Startsev, Mendeleev Commun. 1 (1991) 98.
[10] A.I. Boldyrev, V.I. Avdeev, N.N. Bulgakov and I.I. Zakharov, Kinet. Catal. 17 (1976) 706, in Russian.
[11] V.A. Rabinovich and Z.Ya. Khavin, in: *Brief Handbook of Chemistry*, eds. A.A. Potekhina and A.I. Efimova (Khimiya Edition, Leningrad, 1978) p. 36; *Handbook on Properties of the Elements*, Vol. 1, ed. G.V. Samsonov (Metallurgiya Edition, Moscow, 1976) p. 156.
[12] V.I. Vedeneev, L.V. Gurvich, V.N. Kondratyev, V.A. Medvedev and E.L. Frankevich, in: *Energy of Chemical Bonds Dissociation. Ionization Potentials and Affinity to Electron*, ed. V.N. Kondratyev (AN SSSR Edition, Moscow, 1962) p. 144.
[13] M.Kh. Karapetyants and M.L. Karapetyants, in: *Basic Thermodynamic Constants of Inorganic and Organic Materials* (Khimiya Edition, Moscow, 1968) p. 225.
[14] H.J. Borg, J.F.C.-J.M. Reijerse, R.A. van Santen and J.W. Niemantsverdriet, J. Chem. Phys. 101 (1994) 10052.
[15] Z. Knor, Surf. Sci. 154 (1985) L233.
[16] V.V. Gorodetskii, B.E. Nieuwenhuys, V.M. Sachtler and G.K. Boreskov, Surf. Sci. 108 (1981) 225.
[17] A. Crucq, G. Lienard, L. Degols and A. Frennet, Appl. Surf. Sci. 17 (1983) 79.
[18] V.V. Gorodetskii, V.A. Sobyanin, A.R. Cholach and M.Yu. Smirnov, in: *Proc. 8th ICC*, Vol. 3, Berlin 1984, pp. 323–334.
[19] A.R. Cholach and V.A. Sobyanin, React. Kinet. Catal. Lett. 26 (1984) 381.
[20] K. Tanaka, T. Yamada and B.E. Nieuwenhuys, Surf. Sci. 242 (1991) 503.
[21] R.M. Wolf, J.W. Bakker and B.E. Nieuwenhuys, Surf. Sci. 246 (1991) 135.
[22] M. Kiskinova, S. Lizzit, G. Comelli, G. Paolucci and R. Rosei, Appl. Surf. Sci. 64 (1993) 185.
[23] M. Gierer, F. Mertens, H. Over, G. Ertl and R. Imbihl, Surf. Sci. 339 (1995) L903.
[24] P.W. Murray, F.M. Leibsle, G. Thornton, M. Bowker, V.R. Dhanak, A. Baraldi, M. Kiskinova and R. Rosei, Surf. Sci. 304 (1994) 48.
[25] N.M.H. Janssen, A.R. Cholach, M. Ikai, K. Tanaka and B.E. Nieuwenhuys, Surf. Sci., accepted.
[26] A.G. Makeev, M.M. Slinko, N.M.H. Janssen and P.D. Cobden, J. Chem. Phys. 105 (1996) 7210.
[27] P.D. Cobden, N.M.H. Janssen, Y. van Breugel and B.E. Nieuwenhuys, Surf. Sci. 366 (1996) 432.